Distributed Collaborative Beamforming Design for Maximized Throughput in Real-World Environments

Slim Zaidi, *Student Member*, *IEEE*, and Sofiène Affes, *Senior Member*, *IEEE*

***Abstract*—In this paper, we consider a collaborative beamforming (CB) technique to achieve a dual-hop communication from a source surrounded by M_I interferences to a receiver, through a wireless network comprised of K independent terminals. The CB weights are designed so as to minimize the interferences plus noises' powers while maintaining the received power from the source to a constant level. We show, however, that they are intractable in closed-form due to the complexity of the polychromatic channels arising from the presence of scattering in real-world environments. By recurring to a two-ray channel approximation proved valid at relatively low angular spread (AS) values, we are able to derive the new optimum weights and prove that they could be locally computed at each terminal, thereby complying with the distributed feature of the network of interest. The so-obtained bichromatic distributed collaborative beamforming (B-DCB) is then analyzed and compared in performance to the monochromatic CB (MCB), whose design does not account for scattering, and the optimal CSI-based CB (OCB). It is shown that the proposed B-DCB outperforms its counterparts in real-world environments.**

***Index Terms*—Distributed collaborative beamforming, scattering, angular distribution/spread, interference, wireless sensor networks (WSN).**

I. Introduction

The widely used CB solution that is able to handle both scattering and interference, both present in almost all real-world scenarios, is the optimal CSI-based CB (OCB) [1]-[4]. When the latter is implemented in the network, it has been shown that each collaborating terminal's weight then depends not only on that terminal's CSI, but also on the other terminals' CSI [1]-[4] [5] [6]. Since terminals are very often autonomous and located at different physical locations, they have limited knowledge about each other's CSI. To compute their respective interdependent weights, they have to exchange their local information resulting inevitably in an undesired overhead. The latter increases with the terminals' number K, the interferences' number M_I as well as the channel Doppler frequencies [5] [6]. If one of these parameters is large, this overhead becomes prohibitive and may cause substantial performance degradation and severe terminals' power depletion. This critical impediment motivates further investigation of strategies able to reduce the overhead incurred by OCB.

As such, the optimized CSI or weights' quantization schemes such as the Grassmannian scheme in [7] appear to be efficient strategies to achieve this goal. Nevertheless, the latter usually require a huge codebook that increases the overall cost of the network if integrated at each terminal. Furthermore, the quantization itself introduces errors in weights, thereby causing a CB's performance degradation. More importantly, such schemes do not significantly reduce overhead since the latter still keeps increasing with K, M_I, and channel Doppler frequencies. Another strategy to circumvent this problem consists in ignoring scattering and assuming instead monochromatic (i.e, single-ray) channels. This assumption allows terminals to avoid CSI estimation since the latter will then only depend on each terminal's location and the source and interference DoAs [8]. Several monochromatic CBs (MCB)s have been proposed [8]- [11], but unfortunately shown [12] [13] to perform poorly over polychromatic (i.e., multi-ray) channels due to mismatch. At very small values of the angular spread (AS), the latter results into slight deterioration that becomes, however, quickly unsatisfactory at moderate to large AS. In other words, any overhead gain of MCB against OCB can be achieved only at the expense of some performance loss. Furthermore, this gain is far from being sufficient since MCB's overhead remains linearly dependent on K and M_I. This work aims precisely to develop a new CB solution that approaches the OCB's high performance level at an overhead-cost much lower than the MCB's overhead.

In this paper, we consider an OCB design to achieve a dual-hop communication from a source surrounded by M_I interferences to a receiver, through a wireless network comprised of K independent terminals. The CB weights are designed so as to minimize the interferences plus noises' powers while maintaining the received power from the source to a constant level. We show, however, that they are intractable in closed-form due to the complexity of the polychromatic channels arising from the presence of scattering in real-world environments. By recurring to a two-ray channel approximation proved valid at relatively low angular spread (AS) values, we are able to derive the new optimum weights and prove that they could be locally computed at each terminal, thereby complying with the distributed feature of the network of interest. It is shown that the so-obtained bichromatic distributed collaborative beamforming (B-DCB) outperforms in real-world environments both OCB and MCB.

II. System model

As illustrated in Fig. 1, the system of interest consists of a wireless network or subnetwork comprised of K terminals equipped each with a single isotropic antenna and uniformly and independently distributed on $D(O,R)$, the disc with center at O and radius R, a receiver Rx, and M far-field sources including a desired source $S_{\rm d}$ and M_I interfering sources. All sources are located in the same plane containing $D(O,R)$ [8] [9]. We assume that there is no direct link from the latters to the receiver due to high pathloss attenuation. Moreover, let (r_k,ψ_k) denote the polar coordinates of the k-th terminal and (A_m,ϕ_m) those of the m-th source. Without loss of generality, (A_1,ϕ_1) is assumed to be the location of $S_{\rm d}$ with $\phi_1=0$. Since the sources are in the far-field, we hence assume that $A_m \gg R$ for $m=1,\ldots,M$ where $M=M_I+1$. The following assumptions are further adopted

Work supported by the CRD, DG, and CREATE PERSWADE Programs of NSERC and a Discovery Accelerator Supplement Award from NSERC.

978-1-4799-5952-5/15/$31.00 ©2015 IEEE

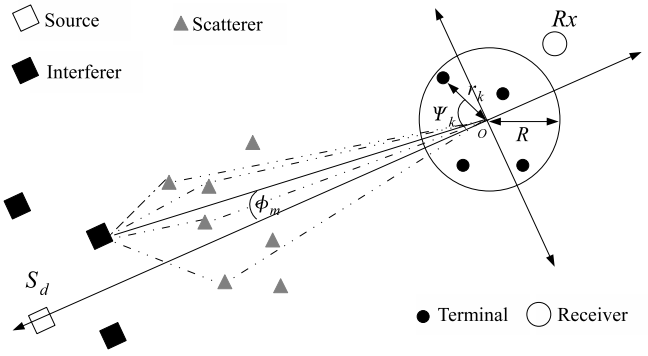

Fig. 1. System model.

throughout this paper:

A1) The m-th source is scattered by a given number of scatterers located in the same plane containing $D(O,R)$. The latter generate from the transmit signal L_m rays or "spatial chromatics" (with reference to their angular distribution) that form a polychromatic propagation channel [12]-[14]. The l-th ray or chromatic is characterized by its angle deviation $\theta_{l,m}$ from the m-th source direction ϕ_m and its complex amplitude $\alpha_{l,m}$. The $\theta_{l,m},\ l=1,\ldots,L$ are i.i.d. zero-mean random variables with a symmetric probability density function (pdf) $p_m(\theta)$ and variance σ_m^2. Note that the standard deviation σ_m is commonly known as the angular spread (AS) while $p_m(\theta)$ is called the scattering or angular distribution [12]-[14]. The $\alpha_{l,m}\ l=1,\ldots,L$ are i.i.d zero-mean random variables with $\mathrm{E}\left\{|\alpha_{l,m}|^2\right\}=1/L_m$. All $\theta_{l,m}$ and $\alpha_{l,m}$ for $m=1,\ldots,M$ and $l=1,\ldots,L_m$ are assumed to be mutually independent.

A2) The forward channel gain $[\mathbf{f}]_k$ from the k-th terminal to the receiver is a zero-mean unit-variance circular Gaussian random variable [13].

A3) The m-th source's signal s_m is narrow-band zero-mean random variable with power p_m while noises at terminals and the receiver are zero-mean Gaussian random variables with variances $\sigma_{n_t}^2$ and $\sigma_{n_r}^2$, respectively. All signals, noises, and the terminals' forward channel gains are mutually independent.

A4) The k-th terminal is only aware of its own coordinates (r_k,ψ_k), its forward channel $[\mathbf{f}]_k$, K, the wavelength λ while being oblivious to the locations and the forward channels of *all* other terminals in the network.

Recurring to A1 and the fact that $A_m \gg R$ for $m=1,\ldots,M$, the backward channel gain from the m-th source to the k-th terminal can be represented as $[\mathbf{g}_m]_k = \sum_{l=1}^{L_m}\alpha_{l,m}e^{-j\frac{2\pi}{\lambda}r_k\cos(\phi_m+\theta_{l,m}-\psi_k)}$. Obviously, when the scattering effect is neglected (i.e., $\sigma_m \longrightarrow 0$) to assume a monochromatic plane-wave propagation channel, we have $\theta_{l,m}=0$ and, hence, $[\mathbf{g}_m]_k$ could be reduced to $\left[\mathbf{g}_m^{(1)}\right]_k = e^{-j(2\pi/\lambda)r_k\cos(\phi_m-\psi_k)}$, the well-known steering vector element in the array-processing literature [8]-[13].

The communication link between the desired source S_{d} and the receiver is established using the following dual-hop scheme. In the first time slot, all sources send their signals to the wireless network while, in the second time slot, the k-th terminal multiplies its received signal with the complex conjugate of its beamforming weight w_k and forwards the resulting signal to the receiver Rx. It can be readily shown that the desired power $P_{\mathbf{w},d}$ received from S_{d} and the undesired power $P_{\mathbf{w},u}$ from both the interference and noise are, respectively, given at the receiver by

$$P_{\mathbf{w},d} = p_1\mathbf{w}^H\mathrm{E}\left\{\mathbf{h}_1\mathbf{h}_1^H\right\}\mathbf{w}, \quad (1)$$

$$P_{\mathbf{w},u} = \mathbf{w}^H\mathrm{E}\left\{\mathbf{H}_{\bar{1}}\mathbf{P}_{\bar{1}}\mathbf{H}_{\bar{1}}^H\right\}\mathbf{w}+\sigma_{n_t}^2\mathbf{w}^H\mathbf{\Sigma}\mathbf{w}+\sigma_{n_r}^2, \quad (2)$$

where $\mathbf{H}_{\bar{1}} \triangleq [\mathbf{f}\odot\mathbf{g}_2\ldots\mathbf{f}\odot\mathbf{g}_M]$ with $\mathbf{f}\triangleq[[\mathbf{f}]_1\ldots[\mathbf{f}]_K]^T$, $\mathbf{P}_{\bar{1}}\triangleq\mathrm{diag}\{p_2\ldots p_M\}$, $\mathbf{\Sigma}\triangleq\mathrm{diag}\{|[\mathbf{f}]_1|^2\ldots|[\mathbf{f}]_k|^2\}$, and $\mathbf{w}\triangleq[w_1,\ldots w_K]$. Note that the expectations in (1) and (2) are taken with respect to the rays' directions $\theta_{l,m}$s and their complex amplitudes $\alpha_{l,m}$s. Although several approaches can be adopted to properly design the beamforming weights, we are only concerned in this paper with the one which minimizes the undesired power $P_{\mathbf{w},u}$ while maintaining the desired power $P_{\mathbf{w},d}$ equal to p_1 []. Mathematically speaking, we have to solve the following optimization problem:

$$\min_{\mathbf{w}}\ \mathbf{w}^H\mathrm{E}\left\{\mathbf{H}_{\bar{1}}\mathbf{P}_{\bar{1}}\mathbf{H}_{\bar{1}}^H\right\}\mathbf{w}+\sigma_{n_t}^2\mathbf{w}^H\mathbf{\Sigma}\mathbf{w}+\sigma_{n_r}^2$$
$$\text{s.t}\quad \mathbf{w}^H\mathrm{E}\left\{\mathbf{h}_1\mathbf{h}_1^H\right\}\mathbf{w}=1, \quad (3)$$

or, equivalently,

$$\max_{\mathbf{w}}\frac{\mathbf{w}^H\mathrm{E}\left\{\mathbf{h}_1\mathbf{h}_1^H\right\}\mathbf{w}}{\mathbf{w}^H\left(\mathrm{E}\left\{\mathbf{H}_{\bar{1}}\mathbf{P}_{\bar{1}}\mathbf{H}_{\bar{1}}^H\right\}+\sigma_{n_t}^2\mathbf{\Sigma}\right)\mathbf{w}}$$
$$\text{s.t.}\quad \mathbf{w}^H\mathrm{E}\left\{\mathbf{h}_1\mathbf{h}_1^H\right\}\mathbf{w}=1. \quad (4)$$

It is straightforward to show that the optimum solution of (4) is a scaled version of the principal eigenvector of the matrix $\left(\mathrm{E}\left\{\mathbf{H}_{\bar{1}}\mathbf{P}_{\bar{1}}\mathbf{H}_{\bar{1}}^H\right\}+\sigma_{n_t}^2\mathbf{\Sigma}\right)^{-1}\mathrm{E}\left\{\mathbf{h}\mathbf{h}^H\right\}$ so as to satisfy the constraint in (4). To the best of our knowledge, this eigenvector cannot be obtained in a closed-form but could be numerically evaluated. However, besides being computationally demanding, this task must be performed by a central processor with global knowledge of all network parameters. The considered network lacks, unfortunately, such a processor.

III. Proposed CB solution

In this section, we prove under mild conditions that it is possible to derive an optimal solution of (4) in closed-form. To this end, we exploit useful approximations of the matrices $\mathrm{E}\left\{\mathbf{h}_1\mathbf{h}_1^H\right\}$ and $\mathrm{E}\left\{\mathbf{H}_{\bar{1}}\mathbf{P}_{\bar{1}}\mathbf{H}_{\bar{1}}^H\right\}$ that have the additional benefit of reducing by the same token the complexity of our CB optimization problem. As such, recurring to assumption A1, we have

$$\mathrm{E}\left\{\mathbf{h}_m\mathbf{h}_m^H\right\}=\int_{\Theta_m}p_m(\theta)\mathbf{a}(\phi_m+\theta)\mathbf{a}^H(\phi_m+\theta)d\theta, \quad (5)$$

where $\mathbf{a}(\theta)\triangleq[[\mathbf{a}(\theta)]_1\ldots[\mathbf{a}(\theta)]_K]^T$ with $[\mathbf{a}(\theta)]_k = [\mathbf{f}]_k e^{-j(2\pi/\lambda)r_k\cos(\theta-\psi_k)}$ and Θ_m is the span of the pdf $p_m(\theta)$ over which the integral is calculated. When the AS σ_m is relatively small, small angular deviations of $\theta_{l,m}$s occur and, hence, the Taylor series expansion of $\mathbf{a}(\phi_m+\theta)$ at ϕ_m yields

$$\mathbf{a}(\phi_m+\theta)\simeq\mathbf{a}(\phi_m)+\mathbf{a}'(\phi_m)\theta+\mathbf{a}''(\phi_m)\frac{\theta^2}{2}, \quad (6)$$

In the Gaussian and Uniform distribution cases, $\Theta_m=[-\inf,+\inf]$ and $\Theta_m=[-\sqrt{3}\sigma_{\theta m},+\sqrt{3}\sigma_{\theta m}]$, respectively.

This condition is assumed for the sole sake of mathematical rigor, without imposing any limitation on AS values in absolute terms. Simulations in Section V will later suggest that practical AS values as high as 17 degrees still keep the following developments valid.

where $\mathbf{a}'(\theta)$ and $\mathbf{a}''(\theta)$ are, respectively, the first and the second derivatives of $\mathbf{a}(\theta)$. After substituting (6) in (5) and integrating in the latter, we have

$$\mathrm{E}\left\{\mathbf{h}_m\mathbf{h}_m^H\right\}\simeq\frac{\mathbf{a}(\phi_m+\sigma_m)\mathbf{a}(\phi_m+\sigma_m)^H+\mathbf{a}(\phi_m-\sigma_m)\mathbf{a}(\phi_m-\sigma_m)^H}{2}, \tag{7}$$

It is noteworthy that the result in (7) also holds with strict equality in the case of bichromatic (i.e., two-ray) channels (i.e., $L_m=2$) with rays located at angles σ_m and $-\sigma_m$ where the channel gain from the m-th source to the k-th terminal is

$$\left[\mathbf{g}_m^{(2)}\right]_k=\alpha_{1,m}e^{-j\frac{2\pi}{\lambda}r_k\cos(\phi_m+\sigma_m-\psi_k)}+\alpha_{2,m}e^{-j\frac{2\pi}{\lambda}r_k\cos(\phi_m-\sigma_m-\psi_k)}. \tag{8}$$

Consequently, when the AS is typically small to moderate, the polychromatic channel $\mathbf{g}_m$ could be substituted with the bichormatic channel $\mathbf{g}_m^{(2)}$. It holds from (7) that $\mathrm{E}\left\{\mathbf{h}_1\mathbf{h}_1^H\right\}=\frac{1}{2}\mathbf{\Xi}$ and $\mathrm{E}\left\{\mathbf{H}_{\bar{1}}\mathbf{P}_{\bar{1}}\mathbf{H}_{\bar{1}}^H\right\}\mathbf{\Gamma}\mathbf{\Lambda}\mathbf{\Gamma}^H$ where $\mathbf{\Xi}=\mathbf{a}(\sigma_1)\mathbf{a}(\sigma_1)^H+\mathbf{a}(-\sigma_1)\mathbf{a}(-\sigma_1)^H$, $\mathbf{\Gamma}=\left[\mathbf{a}(\tilde{\phi}_3),\mathbf{a}(\tilde{\phi}_4),\ldots,\mathbf{a}(\tilde{\phi}_{2M})\right]$ with $\tilde{\phi}_m=\phi_{m/2}-\sigma_{m/2}$ if m is even and $\tilde{\phi}_m=\phi_{(m-1)/2+1}+\sigma_{(m-1)/2+1}$ if m is odd, and $\mathbf{\Lambda}=(1/2)\left[p_2,p_2,\ldots,p_M,p_M\right]$. Therefore, when $\sigma_m,\ m=1,\ldots,M$ are relatively small, (4) could be rewritten as

$$\max_{\boldsymbol{\gamma}}\frac{\boldsymbol{\gamma}^H\tilde{\mathbf{\Xi}}\boldsymbol{\gamma}}{\boldsymbol{\gamma}^H\boldsymbol{\gamma}}\quad\text{s.t.}\quad\boldsymbol{\gamma}^H\tilde{\mathbf{\Xi}}\boldsymbol{\gamma}=2, \tag{9}$$

where $\boldsymbol{\gamma}=\mathbf{\Delta}^{\frac{1}{2}}\mathbf{w}$, $\mathbf{\Delta}=\mathbf{\Gamma}\mathbf{\Lambda}\mathbf{\Gamma}^H+\sigma_{n_t}^2\mathbf{\Sigma}$, and $\tilde{\mathbf{\Xi}}=\mathbf{\Delta}^{-\frac{1}{2}}\mathbf{\Xi}\mathbf{\Delta}^{-\frac{1}{2}}$. It is straightforward to show that the optimum solution of (9) is the principal eigenvector of the matrix $\tilde{\mathbf{\Xi}}$ scaled to satisfy the constraint in (9). Since $\mathbf{\Delta}^{-\frac{1}{2}}$ is a full-rank matrix, $\tilde{\mathbf{\Xi}}$ has the same rank as $\mathbf{\Xi}$ that is inferior or equal to two. Therefore, $\tilde{\mathbf{\Xi}}$ has at most two eigenvectors. In the sequel, we will prove that both $\mathbf{\Delta}^{-\frac{1}{2}}\left(\mathbf{a}(\sigma_1)+\mathbf{a}(-\sigma_1)\right)$ and $\mathbf{\Delta}^{-\frac{1}{2}}\left(\mathbf{a}(\sigma_1)+\mathbf{a}(-\sigma_1)\right)$ are eigenvectors of $\tilde{\mathbf{\Xi}}$. First, let us use the matrix inversion lemma to break $\mathbf{\Delta}^{-1}$ into several terms and, hence, obtain

$$\begin{aligned}&\tilde{\mathbf{\Xi}}\mathbf{\Delta}^{-\frac{1}{2}}\left(\mathbf{a}(\sigma_1)\pm\mathbf{a}(-\sigma_1)\right)=\frac{K}{\sigma_{n_t}^2}\times\\&\Big(\mathbf{\Delta}^{-\frac{1}{2}}\mathbf{a}(\sigma_1)\Big(1+\chi-\boldsymbol{\chi}(\sigma_1)^H\mathbf{D}^{-1}\Big(\boldsymbol{\chi}(\sigma_1)+\boldsymbol{\chi}(-\sigma_1)\Big)\Big)\pm\\&\mathbf{\Delta}^{-\frac{1}{2}}\mathbf{a}(-\sigma_1)\Big(1+\chi^*-\boldsymbol{\chi}(-\sigma_1)^H\mathbf{D}^{-1}\Big(\boldsymbol{\chi}(\sigma_1)+\boldsymbol{\chi}(-\sigma_1)\Big)\Big)\Big),\end{aligned} \tag{10}$$

where $\chi=\left(\mathbf{a}^H(\sigma_1)\mathbf{\Sigma}^{-1}\mathbf{a}(-\sigma_1)\right)/K$, $\boldsymbol{\chi}(\theta)=\left(\mathbf{\Gamma}^H\mathbf{\Sigma}^{-1}\mathbf{a}(\theta)\right)/K$, and $\mathbf{D}=\left(\sigma_{n_t}^2\mathbf{\Lambda}^{-1}+\mathbf{\Gamma}^H\mathbf{\Sigma}^{-1}\mathbf{\Gamma}\right)/K$. Now, we introduce the important theorem below.

Theorem 1: When the number of terminals K is relatively large, we have

$$\mathbf{a}(x)^H\mathbf{\Sigma}^{-1}\mathbf{a}(y)\xrightarrow{p1}2\frac{J_1(\gamma(x-y))}{\gamma(x-y)}, \tag{11}$$

where $\gamma(\phi)\triangleq 4\pi(R/\lambda)\sin(\phi/2)$.

Proof: It follows from the definition of $\mathbf{a}(\theta)$ that $(\mathbf{a}(x)^H\mathbf{\Sigma}^{-1}\mathbf{a}(y))/K=(1/K)\sum_{k=1}^K e^{j\gamma(x-y)z_k}$ where $z_k,\ k=1,\ldots,K$ are i.i.d compound random variables with the pdf $f_{z_k}(z)=\frac{2}{\pi}\sqrt{1-z^2}$ for $-1\le z\le 1$. Using the strong law of large numbers and the fact that $(2/\pi)\int_{-1}^{1}e^{j\gamma(\phi)z}\sqrt{1-z^2}dz=2J_1\left(\gamma\left(\phi\right)\right)/\gamma\left(\phi\right)$, we obtain (11).

It can be then inferred from this theorem that for large K

$$\chi\xrightarrow{p1}2\frac{J_1(\gamma(2\sigma_1))}{\gamma(2\sigma_1)}, \tag{12}$$

$$\boldsymbol{\chi}(\theta)\xrightarrow{p1}2\mathbf{z}(\theta), \tag{13}$$

$$\mathbf{D}\xrightarrow{p1}2\mathbf{Q}, \tag{14}$$

where $\mathbf{Q}$ is a $(2M-2)\times(2M-2)$ matrix with $[\mathbf{Q}]_{mn}=J_1(\gamma(\tilde{\phi}_{m+2}-\tilde{\phi}_{n+2}))/\gamma(\tilde{\phi}_{m+2}-\tilde{\phi}_{n+2})$ if $m\neq n$ and $[\mathbf{Q}]_{mn}=1/2$ otherwise, and $\mathbf{z}(\theta)$ is a $(2M-2)\times 1$ vector with $[\mathbf{z}(\theta)]_m=J_1(\gamma(\theta-\tilde{\phi}_{m+2}))/\gamma(\theta-\tilde{\phi}_{m+2})$ if $\theta\neq\tilde{\phi}_{m+2}$ and $[\mathbf{z}(\theta)]_m=1/2$ otherwise. When $\sigma_m,\ m=1,\ldots,M$ are relatively small, we have $\mathbf{z}(\sigma_1)\simeq\mathbf{z}(-\sigma_1)$ and, hence, it holds from (10)-(14) that, for large K, the eigenvalues associated with $\mathbf{\Delta}^{-\frac{1}{2}}\left(\mathbf{a}(\sigma_1)+\mathbf{a}(-\sigma_1)\right)$ and $\mathbf{\Delta}^{-\frac{1}{2}}\left(\mathbf{a}(\sigma_1)-\mathbf{a}(-\sigma_1)\right)$ are

$$\rho_1(\sigma_1)\simeq\frac{K}{\sigma_{n_t}^2}\left(1+2\frac{J_1(\gamma(2\sigma_1))}{\gamma(2\sigma_1)}-4\mathbf{z}(\sigma_1)^T\mathbf{Q}^{-1}\mathbf{z}(\sigma_1)\right), \tag{15}$$

and

$$\rho_2(\sigma_1)\simeq\frac{K}{\sigma_{n_t}^2}\left(1-2\frac{J_1(\gamma(2\sigma_1))}{\gamma(2\sigma_1)}\right), \tag{16}$$

respectively. What remains to be done to find the principal eigenvector of $\tilde{\mathbf{\Xi}}$ is then comparing the eigenvalues ρ_1 and ρ_2. As such, we introduce the theorem below.

Theorem 2: When the number of terminals K is relatively large, we have

$$2\mathbf{z}(0)^T\mathbf{Q}^{-1}\mathbf{z}(0)\in[0,1[. \tag{17}$$

Proof: It follows from A2 and the results in (11)-(14) that

$$2\mathbf{z}(0)^T\mathbf{Q}^{-1}\mathbf{z}(0)=\lim_{K\to\infty}\frac{1}{K}\|\mathbf{P}\mathbf{a}(0)\|^2, \tag{18}$$

where $\mathbf{P}=\mathbf{\Gamma}(\mathbf{\Gamma}^H\mathbf{\Gamma})^{-1}\mathbf{\Gamma}^H$ is the orthogonal projection matrix onto the subspace spanned by the columns of $\mathbf{\Gamma}$. $\mathbf{P}\mathbf{a}(0)$ is then the projection of $\mathbf{a}(0)$ into the latter subspace and, hence, $0\le 2\mathbf{z}(0)^T\mathbf{Q}^{-1}\mathbf{z}(0)\le\|\mathbf{a}(0)\|=1$. While the left-hand side (LHS) inequality holds with equality if $\mathbf{a}(0)$ is orthogonal to the column span of $\mathbf{\Gamma}$, the right-hand side (RHS) inequality holds with equality if $\mathbf{a}(0)$ is in the column span of $\mathbf{\Gamma}$. The latter event is, however, highly unlikely when K is large and, hence, $2\mathbf{z}(0)^T\mathbf{Q}^{-1}\mathbf{z}(0)$ is strictly inferior to 1.

Using Theorem 2, one can readily show that $\lim_{\sigma_1\to 0}\left(\rho_1-\rho_2\right)(\sigma_1)>0$. Therefore, there exists a real κ such that if σ_1 is small enough we have $\sigma_1<\kappa$ then $\rho_1(\sigma_1)>\rho_2(\sigma_1)$. Consequently, for relatively small $\sigma_m,\ m=1,\ldots,M$ and large K, $\mathbf{\Delta}^{-\frac{1}{2}}\left(\mathbf{a}(\sigma_1)+\mathbf{a}(-\sigma_1)\right)$ is the principal eigenvector of $\tilde{\mathbf{\Xi}}$. Finally, scaling $\mathbf{\Delta}^{-1}(\mathbf{a}(\sigma_1)+\mathbf{a}(-\sigma_1))$ to satisfy the constraint in (9) and using (12)-(14) after breaking $\mathbf{\Delta}^{-1}$ into several terms, we show for relatively small $\sigma_m,\ m=1,\ldots,M$ and large K that the optimal solution of (3) is given by

$$\mathbf{w}_{\mathrm{BD}}=\frac{\mathbf{\Sigma}^{-1}\left(\mathbf{a}\left(\sigma_1\right)+\mathbf{a}\left(-\sigma_1\right)-\mathbf{\Gamma}\mathbf{Q}^{-1}\boldsymbol{\nu}(\sigma_1)\right)}{K\left(1+2\frac{J_1(\gamma(2\sigma_1))}{\gamma(2\sigma_1)}-\boldsymbol{\nu}(\sigma_1)^T\mathbf{Q}^{-1}\boldsymbol{\nu}(\sigma_1)\right)}, \tag{19}$$

where $\boldsymbol{\nu}(\sigma_1)=\mathbf{z}(\sigma_1)+\mathbf{z}(-\sigma_1)$. Note that we denote this CB solution by $\mathbf{w}_{\mathrm{BD}}$ since it relies on the *bichromatic* approximation in (7) and, further, lends itself to a *distributed* implementation, as we will shortly see below. It can be observed from (19)

that the k-th terminal's weight $[\mathbf{w}_{\rm BD}]_k$ depends, according to A4, on the information locally available at this node as well as $\sigma_m,\ m=1,\ldots,M$ and $\phi_m,\ m=1,\ldots,M$, which could be estimated at the sources and broadcasted to the network. Therefore, each terminal is able to autonomously compute its weight without requiring any information exchange with the other terminals in the network. This is in fact a very desired feature for any CB solution since it enables its distributed implementation and, hence, avoids any additional overhead due to such an exchange. Furthermore, from (19), $\mathbf{w}_{\rm BD}$ is independent of $p_m(\theta), m=1,\ldots,M$. This is also an outstanding feature which allows the proposed bichromatic distributed CB (B-DCB)'s implementation in any scattered environment regardless of its scattering distribution.

In the sequel, we compare in performance the proposed B-DCB with the two main conventional types of CB solutions disclosed so far in the literature, namely MCB and OCB (cf. Section I). The first simplifies the optimization by ignoring the presence of scattering and assuming instead monochromatic environments (i.e., $\sigma_m=0,\ m=1,\ldots,M$) and, hence, its beamforming vector is $\mathbf{w}_{\rm M}=\left(\mathbf{A}_{\bar{1}}\mathbf{P}_{\bar{1}}\mathbf{A}_{\bar{1}}^H+\sigma_{n_t}^2\mathbf{\Sigma}\right)^{-1}\mathbf{a}(0)/\mathbf{a}^H(0)\left(\mathbf{A}_{\bar{1}}\mathbf{P}_{\bar{1}}\mathbf{A}_{\bar{1}}^H+\sigma_{n_t}^2\mathbf{\Sigma}\right)^{-1}\mathbf{a}(0)$ where $\mathbf{A}_{\bar{1}}\triangleq[\mathbf{a}(\phi_2)\ldots\mathbf{a}(\phi_M)]$. The second aims to optimize the objective function in (3) without violating its constraint by acting on the instantaneous desired and undesired powers and, therefore, its beamforming vector is $\mathbf{w}_{\rm O}=\left(\mathbf{H}_{\bar{1}}\mathbf{P}_{\bar{1}}\mathbf{H}_{\bar{1}}^H+\sigma_{n_t}^2\mathbf{\Sigma}\right)^{-1}\mathbf{h}_1/\mathbf{h}_1^H\left(\mathbf{H}_{\bar{1}}\mathbf{P}_{\bar{1}}\mathbf{H}_{\bar{1}}^H+\sigma_{n_t}^2\mathbf{\Sigma}\right)^{-1}\mathbf{h}_1$. A straightforward inspection of $\mathbf{w}_{\rm M}$ and $\mathbf{w}_{\rm O}$ reveals that, in contrast with the proposed B-DCB, both MCB and OCB are non-distributed solution whose implementation requires an information exchange among terminals, thereby resulting in an inevitable additional overhead cost.

IV. Performance analysis under real-world conditions

In this section, we analyze and compare in performance the proposed B-DCB with MCB and OCB under real-world conditions (i.e., accounting for implementation errors and the overhead cost).

A. SINR-level CB comparisons

Let $\xi_{\mathbf{w}}$ denote the achieved signal-to-interference-plus-noise ratio (SINR) using $\mathbf{w}$ and given by $\xi_{\mathbf{w}}=\left|\mathbf{w}^H\mathbf{h}_1 s_1\right|^2/\left|\mathbf{w}^H\mathbf{H}_{\bar{1}}\mathbf{s}_{\bar{1}}+\mathbf{w}^H(\mathbf{f}\odot\mathbf{n}_t)+n_r\right|^2$. $\xi_{\mathbf{w}}$ is then an excessively complex function of the random variables n_r, $[\mathbf{n}_t]_k$, r_k, ψ_k and $[\mathbf{f}]_k$ for $k=1,\ldots,K$ and $\alpha_{l,m}$ and $\theta_{l,m}$ $l=1,\ldots,L_m$ for $m=1,\ldots M$ and, hence, a random quantity of its own. Therefore, it is more practical to compare the CB solutions in terms of achieved average-signal-to-average-interference-plus-noise ratio (ASAINR) defined for any $\mathbf{w}$ as $\bar{\xi}_{\mathbf{w}}=p_1\mathrm{E}\left\{\left|\mathbf{w}^H\mathbf{h}_1\right|^2\right\}/\mathrm{E}\left\{\mathbf{w}^H\mathbf{H}_{\bar{1}}\mathbf{P}_{\bar{1}}\mathbf{H}_{\bar{1}}^H\mathbf{w}+\sigma_{n_t}^2\mathbf{w}^H\mathbf{\Sigma}\mathbf{w}\right\}+\sigma_{n_r}^2$. Despite being a more adequate performance metric, please note that the ASINR $\bar{\xi}_{\mathbf{w}}=\mathrm{E}\{\xi_{\mathbf{w}}\}$ cannot be adopted hereafter since, to the best of our knowledge, it appears to be untractable in closed-form.

1) ASAINR gain of B-DCB vs. MCB: From (19), the B-DCB's implementation requires that the m-th source estimates, quantizes and sends $\tilde{\phi}_{2m}$ and $\tilde{\phi}_{2m-1}$, thereby resulting in both angle estimation and quantization errors. In such a case, $[\mathbf{a}(\tilde{\phi}_m)]_k$ should be substituted by $\left[\hat{\mathbf{a}}\left(\tilde{\phi}_m\right)\right]_k=\left[\mathbf{a}\left(\tilde{\phi}_m\right)\right]_k e^{-j\left(\left[\mathbf{e}_{\rm al}\left(\tilde{\phi}_m\right)\right]_k+\left[\mathbf{e}_{\rm aq}\left(\tilde{\phi}_m\right)\right]_k\right)}$ where $\left[\mathbf{e}_{\rm al}(\tilde{\phi}_m)\right]_k$ and $\left[\mathbf{e}_{\rm aq}(\tilde{\phi}_m)\right]_k$ are the angle's localization and quantization errors, respectively. Assuming that these errors are relatively small and recurring to the Taylor's series expansion, one can readily prove that

$$\left[\hat{\mathbf{a}}\left(\tilde{\phi}_m\right)\right]_k\simeq\left[\mathbf{a}\left(\tilde{\phi}_m\right)\right]_k+\left[\mathbf{e}_{\rm a}\left(\tilde{\phi}_m\right)\right]_k, \tag{20}$$

where $\left[\mathbf{e}_{\rm a}(\tilde{\phi}_m)\right]_k=-j\left[\mathbf{a}(\tilde{\phi}_m)\right]_k\left(\left[\mathbf{e}_{\rm al}(\tilde{\phi}_m)\right]_k+\left[\mathbf{e}_{\rm aq}(\tilde{\phi}_m)\right]_k\right)$ with variance $\sigma_{e_{\rm a}}^2=\sigma_{\rm al}^2+\sigma_{\rm aq}^2$. Using a $(B_{\rm a}+1)$-bit uniform quantization, one can easily show that $\sigma_{\rm aq}^2=2^{-2B_{\rm s}}\frac{\pi^2}{12}$. On the other hand, to define $\sigma_{\rm al}^2$, we exploit the CRLB developed in [15] and, hence, $\sigma_{\rm al}^2=\frac{4\sin^2\left(\frac{\pi}{K}\right)\sigma_{n_t}^2}{NK\pi^2}$ where N is the number of samples used to estimate the angle. Using (20), Theorem 1, and the fact that $\left[\mathbf{e}_{\rm al}(\tilde{\phi}_m)\right]_k$s and $\left[\mathbf{e}_{\rm aq}(\tilde{\phi}_m)\right]_k$s are zero-mean i.i.d random variables, we obtain for large K that

$$\hat{\chi}\ \xrightarrow{p1}\ 1+2\frac{J_1(\gamma(2\sigma_1))}{\gamma(2\sigma_1)}+2\sigma_{e_{\rm a}}^2, \tag{21}$$

$$\hat{\boldsymbol{\chi}}(\pm\sigma_1)\ \xrightarrow{p1}\ 2\mathbf{z}(\pm\sigma_1), \tag{22}$$

$$\hat{\mathbf{D}}\ \xrightarrow{p1}\ 2\hat{\mathbf{Q}}, \tag{23}$$

where $\hat{\chi}=\left(\left(\hat{\mathbf{a}}(\sigma_1)+\hat{\mathbf{a}}(-\sigma_1)\right)^H\mathbf{\Sigma}^{-1}\hat{\mathbf{a}}(\sigma_1)\right)/K$, $\hat{\mathbf{Q}}=\mathbf{Q}+\frac{\sigma_{e_{\rm a}}^2}{2}\mathbf{I}_{2M-2}$, $\hat{\boldsymbol{\chi}}(\theta)=\left(\hat{\mathbf{\Gamma}}^H\mathbf{\Sigma}^{-1}\hat{\mathbf{a}}(\theta)\right)/K$, and $\hat{\mathbf{D}}=\left(\mathbf{\Lambda}^{-1}+\hat{\mathbf{\Gamma}}^H\mathbf{\Sigma}^{-1}\hat{\mathbf{\Gamma}}\right)/K$ with $\hat{\mathbf{\Gamma}}=\left[\hat{\mathbf{a}}(\tilde{\phi}_3),\hat{\mathbf{a}}(\tilde{\phi}_4),\ldots,\hat{\mathbf{a}}(\tilde{\phi}_{2M-1}),\hat{\mathbf{a}}(\tilde{\phi}_{2M})\right]$. It follows then from (21)-(23) that the proposed B-DCB is given under real-word conditions by

$$\hat{\mathbf{w}}_{\rm BD}=\frac{\mathbf{\Sigma}^{-1}\left(\hat{\mathbf{a}}\left(\sigma_1\right)+\hat{\mathbf{a}}\left(-\sigma_1\right)-\hat{\mathbf{\Gamma}}\hat{\mathbf{E}}^{-1}\boldsymbol{\nu}(\sigma_1)\right)}{K\left(1+2\frac{J_1(\gamma(2\sigma_1))}{\gamma(2\sigma_1)}+2\sigma_{e_{\rm a}}^2-\boldsymbol{\nu}(\sigma_1)^T\hat{\mathbf{E}}^{-1}\boldsymbol{\nu}(\sigma_1)\right)}. \tag{24}$$

Using the fact that $\hat{\mathbf{Q}}^{-1}\simeq\mathbf{Q}^{-1}-(\sigma_{e_{\rm a}}^2/2)\mathbf{Q}^{-2}$ for small $\sigma_{e_{\rm a}}^2$, we prove that the achieved ASIANR using $\hat{\mathbf{w}}_{\rm BD}$ is given as shown on the top of the next page. When all sources are sufficiently far apart to satisfy

$$\gamma\left(\tilde{\phi}_m-\tilde{\phi}_n\right)\gg\frac{3}{4}\quad m,n=1,\ldots,2M,\quad m\neq n, \tag{26}$$

then we have

$$\frac{J_1\left(\gamma\left(\tilde{\phi}_m-\tilde{\phi}_n\right)\right)}{\gamma\left(\tilde{\phi}_m-\tilde{\phi}_n\right)}=\sqrt{\frac{2}{\pi}}\frac{\cos\left(\gamma\left(\tilde{\phi}_m-\tilde{\phi}_n\right)-\frac{3\pi}{4}\right)}{\gamma\left(\tilde{\phi}_m-\tilde{\phi}_n\right)}, \tag{27}$$

and, hence, $[\boldsymbol{\nu}(\sigma_1)]_m\simeq 0,\ m=1,\ldots,2M$. Therefore, (25) boils down to

$$\tilde{\xi}_{\hat{\mathbf{w}}_{\rm BD}}=\frac{p1\left(1+\frac{2(K-1)\int_{\Theta_1}p_1(\theta)\left(\frac{J_1(\gamma(\theta+\sigma_1))}{\gamma(\theta+\sigma_1)}+\frac{J_1(\gamma(\theta-\sigma_1))}{\gamma(\theta-\sigma_1)}\right)^2d\theta}{\left(1+2\frac{J_1(\gamma(2\sigma_1))}{\gamma(2\sigma_1)}+2\sigma_{e_{\rm a}}^2\right)}\right)}{\sum_{m=2}^M p_m+\sigma_{n_t}^2+\frac{K\sigma_{n_r}^2}{2}\left(1+2\frac{J_1(\gamma(2\sigma_1))}{\gamma(2\sigma_1)}+2\sigma_{e_{\rm a}}^2\right)}. \tag{28}$$

$$\tilde{\xi}_{\hat{\mathbf{w}}_{\mathrm{BD}}}=\frac{p_1\left(1+\frac{\left(2\sigma_{e_{\mathrm{a}}}^2\boldsymbol{\nu}(\sigma_1)^T\hat{\mathbf{Q}}^{-1}\boldsymbol{\nu}(\sigma_1)+2(K-1)\left(\Psi(0)+\sigma_{\mathbf{e}}^2\hat{\Psi}(0)\right)\right)}{1+2\frac{J_1(\gamma(2\sigma_1))}{\gamma(2\sigma_1)}+2\sigma_{e_{\mathrm{a}}}^2-\boldsymbol{\nu}(\sigma_1)^T\hat{\mathbf{Q}}^{-1}\boldsymbol{\nu}(\sigma_1)}\right)}{\sum_{m=2}^{M}p_m\left(1+\frac{2\sigma_{e_{\mathrm{a}}}^2\boldsymbol{\nu}(\sigma_1)^T\hat{\mathbf{Q}}^{-1}\boldsymbol{\nu}(\sigma_1)+2(K-1)\left(\Psi(\phi_m)+\sigma_{\mathbf{e}}^2\hat{\Psi}(\phi_m)\right)}{1+2\frac{J_1(\gamma(2\sigma_1))}{\gamma(2\sigma_1)}+2\sigma_{e_{\mathrm{a}}}^2-\boldsymbol{\nu}(\sigma_1)^T\hat{\mathbf{Q}}^{-1}\boldsymbol{\nu}(\sigma_1)}\right)+\sigma_{n_t}^2+\frac{K\sigma_{n_r}^2}{2}\left(1+2\frac{J_1(\gamma(2\sigma_1))}{\gamma(2\sigma_1)}+2\sigma_{e_{\mathrm{a}}}^2-\boldsymbol{\nu}(\sigma_1)^T\hat{\mathbf{Q}}^{-1}\boldsymbol{\nu}(\sigma_1)\right)}, \tag{25}$$

where $\hat{\Psi}(\phi_m)=\int_{\Theta_m}p_m(\theta)\mathbf{z}\left(\phi_m+\theta\right)^T\mathbf{Q}^{-2}\boldsymbol{\nu}(\sigma_1)\left(\frac{J_1(\gamma(\phi_m+\theta+\sigma_1))}{\gamma(\phi_m+\theta+\sigma_1)}+\frac{J_1(\gamma(\phi_m+\theta-\sigma_1))}{\gamma(\phi_m+\theta-\sigma_1)}-\mathbf{z}\left(\phi_m+\theta\right)^T\mathbf{Q}^{-1}\boldsymbol{\nu}(\sigma_1)\right)d\theta$.

It follows from (28) that the ASAINR achieved by the proposed B-DCB under real-world conditions decreases with $\sigma_{e_{\mathrm{a}}}^2$, as expected.

As far as MCB's implementation is concerned, it implies that the m-th source only estimates, quantizes, and sends its direction ϕ_m. This process unfortunately results in both angle's estimation and quantization errors and, hence, the MCB solution becomes $\hat{\mathbf{w}}_{\mathrm{M}}=\left(\hat{\mathbf{A}}_{\bar{1}}\mathbf{P}_{\bar{1}}\hat{\mathbf{A}}_{\bar{1}}^H+\boldsymbol{\Sigma}\right)^{-1}\hat{\mathbf{a}}(0)/\hat{\mathbf{a}}^H(0)\left(\hat{\mathbf{A}}_{\bar{1}}\mathbf{P}_{\bar{1}}\hat{\mathbf{A}}_{\bar{1}}^H+\boldsymbol{\Sigma}\right)^{-1}\hat{\mathbf{a}}(0)$ where $\hat{\mathbf{A}}_{\bar{1}}\triangleq[\hat{\mathbf{a}}\left(\phi_2\right)\ldots\hat{\mathbf{a}}\left(\phi_M\right)]$. Using (28), we show if the condition in (26) is satisfied that

$$\hat{\Upsilon}\left(\hat{\mathbf{w}}_{\mathrm{M}}\right)\simeq\frac{\left(1+2\frac{J_1(\gamma(2\sigma_1))}{\gamma(2\sigma_1)}+2\sigma_{e_{\mathrm{a}}}^2\right)^2\int_{\Theta_1}p_1(\theta)\left(\frac{J_1(\gamma(\theta))}{\gamma(\theta)}\right)^2d\theta}{\left(1+\sigma_{e_{\mathrm{a}}}^2\right)^2\int_{\Theta_1}p_1(\theta)\left(\frac{J_1(\gamma(\theta+\sigma_1))}{\gamma(\theta+\sigma_1)}+\frac{J_1(\gamma(\theta-\sigma_1))}{\gamma(\theta-\sigma_1)}\right)^2d\theta}, \tag{29}$$

holds for large K. In (29), $\hat{\Upsilon}\left(\mathbf{w}\right)=\tilde{\xi}_{\mathbf{w}}/\tilde{\xi}_{\hat{\mathbf{w}}_{\mathrm{BD}}}$ and, hence, $\hat{\Upsilon}\left(\hat{\mathbf{w}}_{\mathrm{M}}\right)\simeq 1$ holds when there is no scattering. This is expected since, in such case both, B-DCB and MCB's implementations require M quantized angle estimates and, therefore, equally suffer from their estimation and quantization errors. However, when σ_1 is relatively small, i.e., in lightly- to moderately-scattered environments, the Taylor series expansion of $J_1\left(\gamma\left(\theta\pm\sigma_1\right)\right)/\gamma\left(\theta\pm\sigma_1\right)$ at θ yields

$$\frac{J_1\left(\gamma\left(\theta\pm\sigma_1\right)\right)}{\gamma\left(\theta\pm\sigma_1\right)}=\frac{J_1\left(\gamma\left(\theta\right)\right)}{\gamma\left(\theta\right)}\pm\sigma_1\left(\frac{J_1\left(\gamma\left(x\right)\right)}{\gamma\left(x\right)}\right)'\Big|_{x=\dot{\theta}}, \tag{30}$$

and, hence, $\hat{\Upsilon}\left(\hat{\mathbf{w}}_{\mathrm{M}}\right)$ is reduced to

$$\hat{\Upsilon}\left(\hat{\mathbf{w}}_{\mathrm{M}}\right)\simeq\frac{\left(1+2\frac{J_1(\gamma(2\sigma_1))}{\gamma(2\sigma_1)}+2\sigma_{e_{\mathrm{a}}}^2\right)^2}{4\left(1+\sigma_{e_{\mathrm{a}}}^2\right)^2}. \tag{31}$$

Since $J_1(\gamma(x))/\gamma(x)$ is a decreasing function of x that reach its maximum $1/2$ at $x=0$, $\hat{\Upsilon}\left(\hat{\mathbf{w}}_{\mathrm{M}}\right)$ decreases when σ_1 increases. Consequently, in ideal conditions (i.e., $\sigma_{e_{\mathrm{a}}}^2=0$), the proposed B-DCB outperforms MCB in lightly- to moderately-scattered environments. When σ_1 is large, i.e., in highly-scattered environments, $J_1(\gamma(x))/\gamma(x)\simeq 0$ and, hence, $\hat{\Upsilon}\left(\hat{\mathbf{w}}_{\mathrm{M}}\right)<1$ always holds in ideal conditions. Therefore, the proposed B-DCB outperforms MCB also in highly-scattered environments. However, according to (29), its achieved ASANR gain is reduced when $\sigma_{e_{\mathrm{a}}}^2$ increases, as $1+2J_1(\gamma(2\sigma_1))/\gamma(2\sigma_1)\leq 2$. This is expected since the B-DCB's implementation requires more angular information than MCB and, hence, is more affected by their estimation and quantization errors. In addition from (29), the ASAINR gain of B-DCB against MCB may turn into losses under exceptional circumstances hard to justify in practice (e.g., low quantization level or very small B_{a} which results in large quantization errors and, consequently, in a large $\sigma_{e_{\mathrm{a}}}^2$).

2) ASAINR gain of B-DCB vs. OCB: From $\mathbf{w}_{\mathrm{O}}$'s definition, the OCB's implementation requires that the m-th source estimates and quantizes the channels $[\mathbf{g}_m]_k, k=1\ldots K$ before sending them back to all K terminals, thereby resulting in both estimation and quantization errors. Let us denote the resulting channel between the m-th source and the k-th terminal by $[\hat{\mathbf{g}}_m]_k=[\mathbf{g}_m]_k+[\mathbf{e}_{\mathrm{c,m}}]_k$ where $\mathbf{e}_{\mathrm{c,m}}=\mathbf{e}_{\mathrm{ci,m}}+\mathbf{e}_{\mathrm{cq,m}}$ and $\mathbf{e}_{\mathrm{ci,m}}$ and $\mathbf{e}_{\mathrm{cq,m}}$ are the channel identification and quantization errors, respectively. Let $\sigma_{e_{\mathrm{c}}}^2=\sigma_{\mathrm{ci}}^2+\sigma_{\mathrm{cq}}^2$ be the variance of $[\mathbf{e}_{\mathrm{c,m}}]_k$ where σ_{ci}^2 and σ_{cq}^2 are those of $[\mathbf{e}_{\mathrm{ci,m}}]_k$ and $[\mathbf{e}_{\mathrm{cq,m}}]_k$, respectively. Assuming a $(B_{\mathrm{c}}+1)$-bit uniform quantization, we have $\sigma_{\mathrm{cq}}^2=2^{-2B_{\mathrm{c}}}\frac{g_{\mathrm{Max}}^2}{12}$ where g_{Max} is the peak amplitude of all channels' realizations $[\mathbf{g}_m]_k$ for $k=1,\ldots,K$. Based on [16], we have $\sigma_{\mathrm{ci}}^2=\frac{3}{2}\left(\pi\sigma_{n_t}^2\bar{f}_{\mathrm{D}}\right)^{\frac{2}{3}}$ where $\bar{f}_{\mathrm{D}}$ is the normalized Doppler frequency. Substituting $\mathbf{h}_m$ by $\hat{\mathbf{h}}_m=\mathbf{f}\odot\hat{\mathbf{g}}_m$ in $\mathbf{w}_{\mathrm{O}}$'s expression, we obtain the OCB's beamforming vector $\hat{\mathbf{w}}_{\mathrm{O}}$. Using the fact that $[\mathbf{e}_{\mathrm{c,m}}]_k$s are i.i.d random variables independent from the channels $[\mathbf{g}_m]_k$s, we prove that

$$\tilde{\xi}_{\hat{\mathbf{w}}_{\mathrm{O}}}\simeq\frac{p_1}{\left(1+\sigma_{e_{\mathrm{c}}}^2\right)\sigma_{n_r}^2}, \tag{32}$$

when K is large enough. It follows from (28) and (32) that under ideal conditions, $\hat{\Upsilon}\left(\hat{\mathbf{w}}_{\mathrm{O}}\right)\simeq 1$ holds when σ_1 is small (i.e., lightly- to moderately-scattered environments) while $\hat{\Upsilon}\left(\hat{\mathbf{w}}_{\mathrm{O}}\right)>1$ holds when the latter is large (i.e., in highly-scattered environments). However, according to (25) and (32), the ASAINR gain achieved by OCB against the proposed B-DCB decreases when $\bar{f}_{\mathrm{D}}$ increases (i.e., $\sigma_{e_{\mathrm{c}}}^2$ increases). Therefore, if $\sigma_{e_{\mathrm{a}}}^2$ is sufficiently small, $\hat{\Upsilon}\left(\hat{\mathbf{w}}_{\mathrm{O}}\right)<1$ holds in lightly- to moderately-scattered environments. In such environments, the proposed B-DCB is then able to outperform OCB. Simulations in Section V will later show that this gain translates into a larger operational region in terms of AS values over which B-DCB is favored against OCB. Furthermore, when $\bar{f}_{\mathrm{D}}$ is large enough to satisfy

$$\bar{f}_{\mathrm{D}}>\frac{\left(\frac{2}{3}\left(\left(\sigma_{n_r}^2\tilde{\xi}_{\hat{\mathbf{w}}_{\mathrm{BD}}}\right)^{-1}-1\right)-\sigma_{\mathrm{cq}}^2\right)^{\frac{3}{2}}}{\pi\sigma_{n_t}^2}, \tag{33}$$

then we have from (25) and (32) that $\hat{\Upsilon}\left(\hat{\mathbf{w}}_{\mathrm{O}}\right)<1$ holds for any $p_m(\theta)$ and $\sigma_m, m=1,\ldots,M$. Consequently, under real-world conditions and even in highly-scattered environments, the proposed B-DCB is able to outperform OCB whose performance severely deteriorates at high Doppler. This further proves once again the efficiency of the proposed CB solution.

For both the sake of simplicity and tractability, we recur here to the Uniform quantization of channel estimates which is far from optimal in contrast for instance to the Grassmannian quantization scheme in [7].

B. Link-level throughput CB comparisons

The ASAINR comparisons above, despite their valuable insights, face a major weakness in that they do not factor in the different overhead costs incurred by each CB solution. Hence, comparisons in terms of the link-level throughput become crucial. Assuming without loss of generality BPSK-modulated transmissions, it can be shown for large K that the link-level throughput achieved by $\mathbf{w}$ is given by

$$\mathcal{T}_{\mathbf{w}} \simeq 0.5 \left(R_{\mathrm{T}} - R^{\mathrm{oh}}_{\mathbf{w}}\right) \log_2 \left(1 + \tilde{\xi}_{\mathbf{w}}\right) \tag{34}$$

where R_{T} and $R^{\mathrm{oh}}_{\mathbf{w}}$ are the transmission bit rate and the overhead bit rate allocated to $\mathbf{w}$'s implementation. The throughput gain achieved by any given beamformer $\mathbf{w}$ over the proposed B-DCB solution is therefore given by

$$\mathcal{G}\left(\mathbf{w}\right) = \frac{\mathcal{T}_{\mathbf{w}} - \mathcal{T}_{\hat{\mathbf{w}}_{\mathrm{BD}}}}{\mathcal{T}_{\hat{\mathbf{w}}_{\mathrm{BD}}}}. \tag{35}$$

We will shortly see below, both by analysis and simulations, that this performance metric, despite the simplifying assumptions above, is still able to provide a comparative framework that is extremely insightful qualitatively.

1) Throughput gain of B-DCB vs. OCB: As discussed in Section IV-A1, the proposed B-DCB implementation requires that the m-th source broadcasts $\tilde{\phi}_{2m}$ and $\tilde{\phi}_{2m-1}$. Each angle's broadcast requires one time slot of B_{a} bits transmitted at a localization refreshment rate $f_{\mathrm{LR}} = 1/T_{\mathrm{LR}}$ where T_{LR} is the refreshment period. Since the latter is typically very large, we assume that $f_{\mathrm{LR}} \simeq 0$ and, hence, we have $R^{\mathrm{oh}}_{\mathbf{w}_{\mathrm{BD}}} \simeq 0$. The throughput achieved by the proposed B-DCB is then given by

$$\mathcal{T}_{\hat{\mathbf{w}}_{\mathrm{BD}}} \simeq 0.5 R_{\mathrm{T}} \log_2 \left(1 + \tilde{\xi}_{\hat{\mathbf{w}}_{\mathrm{BD}}}\right). \tag{36}$$

On the other hand, the OCB's implementation requires that the m-th source broadcasts all $[\mathbf{g}_m]_k, k = 1 \ldots K$ for all K terminals. This process requires K time slots of B_{c} bits transmitted at an identification refreshment rate $f_{\mathrm{IR}} = 1/T_{\mathrm{IR}}$ where T_{IR} denotes the refreshment period. It is noteworthy that T_{IR} should satisfy $T_{\mathrm{IR}} \geq T_{\mathrm{c}}$ where $T_{\mathrm{c}} = 0.423/f_{\mathrm{D}}$ is the coherence time and f_{D} is the maximum Doppler frequency. For simplicity, we assume $f_{\mathrm{IR}} = 2f_{\mathrm{D}}$. The overhead rate of such process is then $2KMB_{\mathrm{c}}f_{\mathrm{D}}$. Furthermore, from $\mathbf{w}_{\mathrm{O}}$'s definition, the OCB's implementation requires also that the k-th terminal broadcasts $[\mathbf{f}]_k$ in the network. This is in contrast to the proposed B-DCB whose implementation avoids such information exchange among terminals, thanks to its distributed nature. Assuming that B_{c} bits are allocated to $[\mathbf{f}]_k$ and refreshed every T_{IR}, the OCB's implementation overhead rate is then $R^{\mathrm{oh}}_{\hat{\mathbf{w}}_{\mathrm{O}}} = 2K(M+1)B_{\mathrm{c}}f_{\mathrm{D}}$ and, hence, its achieved throughput is

$$\mathcal{T}_{\hat{\mathbf{w}}_{\mathrm{O}}} = 0.5 R_{\mathrm{T}} \left(1 - 2K(M_I+2)B_{\mathrm{c}}\bar{f}_{\mathrm{D}}\right) \log_2 \left(1 + \tilde{\xi}_{\hat{\mathbf{w}}_{\mathrm{O}}}\right). \tag{37}$$

As can be observed from (37), the throughput achieved by OCB decreases with the number of terminals K as well as the number of interfering sources M_I. Furthermore, since $\tilde{\xi}_{\hat{\mathbf{w}}_{\mathrm{O}}}$ decreases when $\bar{f}_{\mathrm{D}}$ increases, it follows then from the above result that $\tilde{\mathcal{T}}_{\hat{\mathbf{w}}_{\mathrm{O}}}$ also decreases if $\bar{f}_{\mathrm{D}}$ increases. Interestingly, from (37), B_{c} has two contradictory effects on $\tilde{\mathcal{T}}_{\hat{\mathbf{w}}_{\mathrm{O}}}$. Indeed, if B_{c} increases, the OCB overhead rate increases and, hence, $\tilde{\mathcal{T}}_{\hat{\mathbf{w}}_{\mathrm{O}}}$ decreases. However, from (32), increasing B_{c} (i.e., decreasing $\sigma^2_{e_{\mathrm{c}}}$) improves $\tilde{\xi}_{\hat{\mathbf{w}}_{\mathrm{O}}}$ and, therefore, the achieved throughput $\tilde{\mathcal{T}}_{\hat{\mathbf{w}}_{\mathrm{O}}}$. The result in (37) could then be exploited to find the optimum number of quantization bits $B^{\mathrm{opt}}_{\mathrm{c}}$ that maximizes the OCB's throughput. Moreover, since B-DCB's throughput is, in contrast to OCB, independent of K, M_I, and $\bar{f}_{\mathrm{D}}$, from (37) and (36), then $\mathcal{G}\left(\hat{\mathbf{w}}_{\mathrm{O}}\right)$ decreases if one of these parameters increases. Furthermore, if (33) is satisfied, we easily show that $\mathcal{G}\left(\hat{\mathbf{w}}_{\mathrm{O}}\right) < 0$. Simulations in Section V will later show that this result translates into a wider operational region in terms of AS values over which B-DCB is favored against OCB, reaching actually as much as 50 degrees thereby covering about the entire span of AS values.

2) Throughput gain of B-DCB vs. MCB: From $\mathbf{w}_{\mathrm{M}}$'s definition, in order to properly implement MCB, the m-th source must only broadcast its direction ϕ_m to the network and, additionally, terminals must exchange their positions as well as their forward channels. This is in contrast to the proposed B-DCB whose implementation avoids such an exchange due to its distributed nature. Assuming that each position should be refreshed every T_{LR}, which is typically large, it can be readily shown that MCB's implementation overhead rate is $R^{\mathrm{oh}}_{\mathbf{w}_{\mathrm{M}}} = 2Kf_{\mathrm{D}}$ and, therefore,

$$\mathcal{T}_{\hat{\mathbf{w}}_{\mathrm{M}}} \simeq 0.5 R_{\mathrm{T}} \left(1 - 2K\bar{f}_{\mathrm{D}}\right) \log_2 \left(1 + \tilde{\xi}_{\hat{\mathbf{w}}_{\mathrm{M}}}\right). \tag{38}$$

As can be observed from (38), in contrast to the proposed B-DCB, the throughput achieved by MCB decreases when K and/or $\bar{f}_{\mathrm{D}}$ increase/s. Since $\tilde{\xi}_{\hat{\mathbf{w}}_{\mathrm{M}}} \leq \tilde{\xi}_{\hat{\mathbf{w}}_{\mathrm{BD}}}$ for any p_m and $\sigma_m, m = 1, \ldots, M$ for practical values of B_{a}, then $\mathcal{G}\left(\hat{\mathbf{w}}_{\mathrm{O}}\right) \leq 0$ holds. From (36) and (38), this gain decreases with K and f_{D}. Consequently, under real-world conditions, the proposed B-DCB always outperforms MCB in terms of throughput. This also holds true in scattering-free environments (i.e., $\sigma_m = 0$ for $m = 1, \ldots, M$) where MCB and B-DCB achieves the same ASAINR, as proved in Section IV-A1.

V. Simulation Results

Computer simulations are provided to support the theoretical results. All empirical average quantities are calculated over 10^6 random realizations of r_k, ψ_k, $[\mathbf{f}]_k$ for $k = 1, \ldots, K$ and $\alpha_{l,m}$, $\theta_{l,m}$ for $l = 1, \ldots, L_m$. In all simulations, all sources have the same power $p = 1$ and $\sigma^2_{n_r} = \sigma^2_{n_t} = 1$. The number of rays is $L_m = 6$, $\sigma_m = \sigma$ and the scattering distribution $p_m(\theta)$ is Uniform for $m = 1, \ldots, M$. Unless otherwise stated, $K = 20$ and $M_I = 3$ with $[\phi_2, \phi_3, \phi_4] = [10, 15, 20]$ degrees.

Fig. 2 displays the analytical and the empirical ASAINR gains achieved by $\hat{\mathbf{w}}_{\mathrm{M}}$ and $\hat{\mathbf{w}}_{\mathrm{O}}$ against $\hat{\mathbf{w}}_{\mathrm{BD}}$ for different values of σ. Fig. 2(a) plots $\hat{\Upsilon}(\hat{\mathbf{w}}_{\mathrm{M}})$ versus B_{a} for $\sigma \in \{0, 5, 10, 15\}$ degrees while Fig. 2(b) plots $\hat{\Upsilon}(\hat{\mathbf{w}}_{\mathrm{O}})$ versus $\bar{f}_{\mathrm{D}}$ for $\sigma \in \{0, 17, 20, 25\}$ degrees when $B_{\mathrm{a}} = B_{\mathrm{c}} = 8$ bits. From both figures, the analytical results of Section IV-A closely approach the empirical $\hat{\Upsilon}(\hat{\mathbf{w}}_{\mathrm{M}})$ and $\hat{\Upsilon}(\hat{\mathbf{w}}_{\mathrm{O}})$, respectively, for $K = 20$. It can be observed from Fig. 2(a) that $\hat{\Upsilon}(\hat{\mathbf{w}}_{\mathrm{M}}) \simeq 1$ holds regardless of B_{a} when $\sigma = 0$ (i.e., there is no scattering). However, when σ increases, $\hat{\Upsilon}(\hat{\mathbf{w}}_{\mathrm{M}})$ substantially decreases if the quantization level B_{a} is kept sufficiently large. Besides, from this figure, $\hat{\Upsilon}(\hat{\mathbf{w}}_{\mathrm{M}})$ increases if the quantization level B_{a} decreases and even slightly exceeds 1 when B_{a} becomes very small (i.e., $B_{\mathrm{a}} \leq 3$). Therefore, under real-world conditions, the proposed B-DCB always outperforms MCB except at unrealistic low quantization levels which are hard to justify in practice. This corroborates the discussions made in

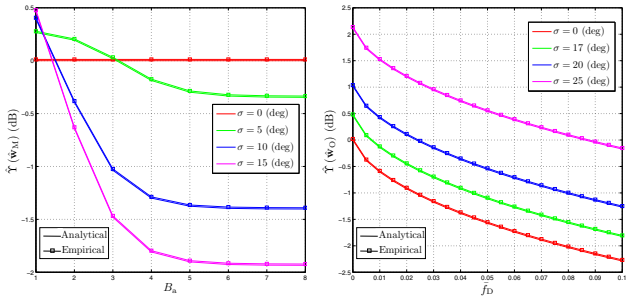

(a) (b)

Fig. 2. The analytical and the empirical ASAINR gains achieved, under real-world conditions, by MCB and OCB against the proposed B-DCB vs. (a): B_a and (b): $\bar{f}_D$, respectively, for $K = 20$ and different values of σ.

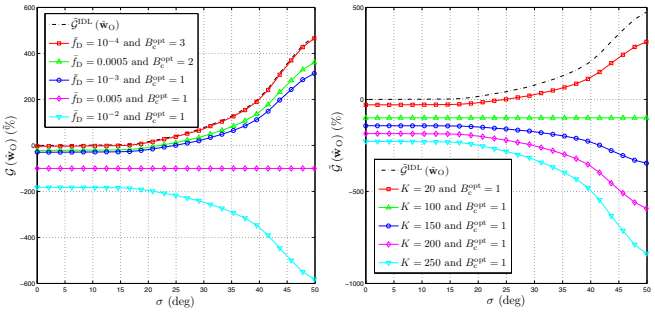

(a) (b)

Fig. 3. The throughput gain $\mathcal{G}(\hat{\mathbf{w}}_O)$ achieved, under real-world conditions, by OCB versus σ for different values of (a): $\bar{f}_D$ at $K = 20$, and (b): K at $\bar{f}_D = 0.001$.

Section IV-A1. As discussed in Section IV-A2, from Fig. 2(b), the ASAINR gain $\hat{\Upsilon}(\hat{\mathbf{w}}_O)$ achieved by OCB against the proposed B-DCB decreases with $\bar{f}_D$. This figure confirms and illustrates the existence of a threshold value of $\bar{f}_D$ beyond which the ASAINR gain achieved by OCB turns into losses. As expected, this threshold whose expression is given by (33) increases with σ, since $\tilde{\xi}_{\hat{\mathbf{w}}_{BD}}$ decreases with the latter. For instance, we find that $\hat{\Upsilon}(\hat{\mathbf{w}}_O) \leq 1$ when $\sigma = 20$ degrees if $\bar{f}_D \geq 0.025$ or when $\sigma = 25$ degrees if $\bar{f}_D \geq 0.087$.

Fig. 3 displays $\mathcal{G}(\hat{\mathbf{w}}_O)$ for different values of $\bar{f}_D$ and K. In this figure, curves are plotted after performing a numerical evaluation of the optimum quantization level B_c^{opt} for each pair of values of $\bar{f}_D$ and K. For instance, we find that $B_c^{opt} = 2$ bits when $\bar{f}_D = 0.0005$ and $K = 20$ while $B_c^{opt} = 1$ bit when $\bar{f}_D = 10^{-3}$ and $K = 200$. From this figure, the OCB's throughput gain against the proposed B-DCB decreases when $\bar{f}_D$ and/or K increase/s. This gain may turn into losses for sufficiently large K and/or high $\bar{f}_D$, even when σ is large. As can be observed from Fig. 3, this result translates into a larger operational region of up to 50 degrees for large K and/or high $\bar{f}_D$ that amounts to angle deviations from almost -90 to 90 degrees (i.e., the entire angular span). Besides, $\mathcal{G}(\hat{\mathbf{w}}_O)$ which is nominally an increasing function of σ under ideal conditions, becomes constant at -100% when $K = 20$ and $\bar{f}_D = 0.005$ or when $K = 100$ and $\bar{f}_D = 0.001$, and even a decreasing function of σ, when K and/or $\bar{f}_D$ are/is large. All these observations corroborate all the elements of our discussion in Section IV-B1.

VI. Conclusions

In this paper, a CB technique aiming to achieve a dual-hop communication from a source surrounded by M_I interferences to a receiver was considered. Its weights were designed so as to minimize the interferences plus noises' powers while maintaining the received power from the source to a constant level. We showed, however, that they are intractable in closed-form due to the complexity of the polychromatic channels arising from the presence of scattering. By recurring to a two-ray channel approximation proved valid at relatively low AS values, we were able to derive the new optimum weights and prove that they could be locally computed at each terminal, thereby complying with the distributed feature of the network of interest. The so-obtained B-DCB was then analyzed and compared in performance to both MCB and OCB. We showed that the proposed B-DCB always outperforms MCB and, further, its performance approaches that of OCB.

References

[1] Y. Jing and H. Jafarkhani, " Network beamforming using relays with perfect channel information," *IEEE Trans. Inf. Theory,* vol. 55, pp. 2499-2517, June 2009.

[2] H. Shen, W. Xu, S. Jin, and C. Zhao, "Joint transmit and receive beamforming for MIMO downlinks with channel uncertainty," *IEEE Trans. Veh. Tech.,* vol. 63, pp. 2319-2335, June 2014.

[3] S. Zaidi, B. Hmidet, and S. Affes, "Power-constrained distributed implementation of SNR-optimal collaborative beamforming in highly-scattered environments," accepted for publicalion in *IEEE Wireless Commun., Lett.,* May 2015.

[4] H.-B. Kong, C. Song, H. Park, and I. Lee, "A new beamforming design for MIMO AF relaying systems with direct link," *IEEE Trans. Commun.,* vol. 62, pp. 2286-2295, July 2014.

[5] S. Zaidi and S. Affes, "SNR and throughput analysis of distributed collaborative beamforming in locally-scattered environments," *Wiley J. Wireless Commun. and Mobile Comput.,* vol. 12, pp. 1620-1633, Dec. 2012. Invited Paper.

[6] S. Zaidi and S. Affes, "Analysis of collaborative beamforming designs in real-world environments," *Proc. IEEE WCNC'2013,* Shanghai, China, Apr. 7-10, 2013.

[7] D. J. Love, R. W. Heath, and T. Strohmer, "Grassmannian beamforming for multiple-input multiple-output wireless systems," *IEEE Trans. Inf. Theory,* vol. 49, pp. 2735-2747, Oct. 2003.

[8] H. Ochiai, P. Mitran, H. V. Poor, and V. Tarokh, "Collaborative beamforming for distributed wireless ad hoc sensor networks," *IEEE Trans. Signal Process.,* vol. 53, pp. 4110-4124, Nov. 2005.

[9] M. F. A. Ahmed and S. A. Vorobyov, "Collaborative beamforming for wireless sensor networks with Gaussian distributed sensor nodes," *IEEE Trans. Wireless Commun.,* vol. 8, pp. 638-643, Feb. 2009.

[10] K. Zarifi, A. Ghrayeb, and S. Affes , "Distributed beamforming for wireless sensor networks with improved graph connectivity and energy efficiency," *IEEE Trans. Signal Process.,* vol. 58, pp. 1904-1921, Mar. 2010.

[11] L. Dong, A. P. Petropulu, and H. V. Poor, "A cross-layer approach to collaborative beamforming for wireless ad hoc networks," *IEEE Trans. Signal Process.,* vol. 56, pp. 2981-2993, July 2008.

[12] A. Amar, "The effect of local scattering on the gain and beamwidth of a collaborative beampattern for wireless sensor networks," *IEEE Trans. Wireless Commun.,* vol. 9, pp. 2730-2736, Sep. 2010.

[13] S. Zaidi and S. Affes "Distributed collaborative beamforming in the presence of angular scattering," *IEEE Trans. Commun.,* vol. 62, pp. 1668-1680, May 2014.

[14] D. Astly and B. Ottersten, "The effects of local scattering on direction of arrival estimation with MUSIC," *IEEE Trans. Signal Process.,* vol. 47, pp. 3220-3234, Dec. 1999.

[15] F. Bellili, S. B. Hassen, S. Affes, and A. Stéphenne, "Cramer-Rao lower bounds of DOA estimates from square QAM-modulated signals," *IEEE Trans. Signal Process.,* vol. 59, pp. 1675-1685, June 2011.

[16] S. Affes and P. Mermelstein, "Adaptive space-time Processing for wireless CDMA," Chap. 10, pp. 283-321, in *Adaptive Signal Processing: Application to Real-World Problems,* J. Benesty and A. H. Huang, Eds., Springer, Berlin, Germany, Feb. 2003.